PERGAMON

Continental Shelf Research 20 (2000) 2325–2345

CONTINENTAL SHELF RESEARCH

The shoreface-connected ridges along the central Dutch coast — part 2: morphological modelling

Jan W.H. van de Meene[a,*], Leo C. van Rijn[a,b]

[a]*Institute for Marine and Atmospheric Research, Utrecht University, P.O. Box 80115, 3508 TC Utrecht, The Netherlands*

[b]*Delft Hydraulics, P.O. Box 177, 2600 MH Delft, The Netherlands*

Received 22 July 1994; received in revised form 1 April 1998; accepted 28 February 2000

Abstract

The long-term (decades, centuries) morphological behaviour of the shoreface-connected ridges along the central Dutch coast was studied with a simplified modelling approach, consisting of a 1D current model (*Trenchflow*), combined with a 2DV morphodynamic model (*Sutrench*). The analysis focused on a cross-section of a single sand bank, assuming that the interaction of the water motion and morphology could be considered a local phenomenon. The modelling was used for a sensitivity analysis of the relevant processes. The present model reveals a positive feedback: the schematized sand bank is predicted to grow, while there is no damping, even not during high waves. However, using the observed flow response, which differs from the theoretical flow response as described in Part 1 of this paper, actual growth rates are close to zero. The modelling shows that the ridges are stable on a time scale of years to decades, while they may be considered active on the time scale of thousands of years. Calculated migration rates of the ridges are in the order of 1 m/yr. Morphological time scale and migration rate correspond to the results from a geological reconstruction.

1. Introduction

Part 1 of this paper (Van de Meene and Van Rijn, 2000) has shown that the theoretical response of the tidal current flowing across the shoreface-connected ridges along the central Dutch coast (Fig. 1) was observed in nature only partially and inconsistently. Possible explanations for the deviations between theory and

*Corresponding author. Present address: Royal Boskalis Westminster NV, P.O. Box 43, 3350 AA Papendrecht, The Netherlands. Tel.: +31-78-6969000; fax +31-78-6969555.

0278-4343/00/$ - see front matter
PII: S0278-4343(00)00049-2

observations were the setting of the ridges (relatively shallow water, close to the coast and connected to the shoreface) and the presence of persistent cross-shore density-driven circulations, possibly overriding the expected flow response. Also, the field measurements did not give a full and long-term coverage of the actual currents in the study area, although they were carried out rather extensively. A review of other field studies revealed that also in other ridge fields the theoretical flow response could not be observed consistently and convincingly. This means that the available field observations do not yet allow for any firm conclusion with respect to the presence in nature of the theoretical flow response. Probably, a much more refined modelling approach is required in order to be able to describe the morphological evolution of ridge fields of the type depicted in Fig. 1 in complicated environments like the inner-shelf. Such morphodynamic modelling, focusing on the lateral coherence of the sand bank systems and taking into account non-linear interactions between the water motion, sediment transport and morphological evolution of the sea bed, is still in an early stage of development (cf. De Vriend et al., 1993; Hulscher et al., 1993; Hulscher, 1996).

Although there is only limited agreement between observations and theory, a simplified modelling approach was adopted in order to obtain a sensitivity analysis of the major processes that may affect the morphological evolution of the ridges. In addition, the applied modelling approach allowed for an evaluation of the effect of

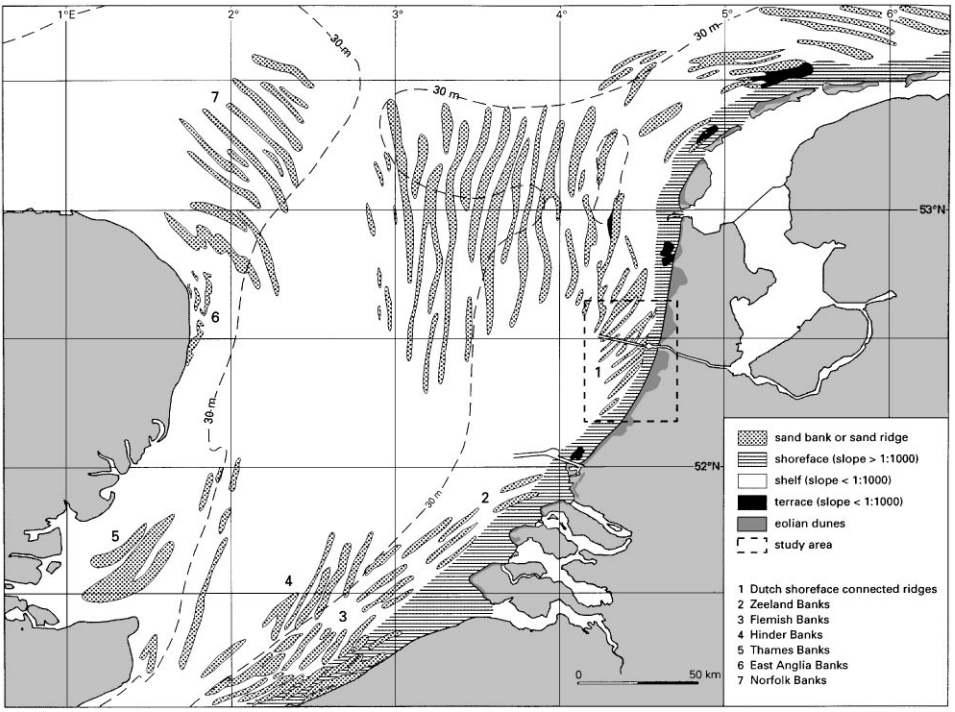

Fig. 1. Linear sand banks in the southern part of the North Sea.

the observed flow response to the morphological development of the ridges. The modelling was done in two steps, starting with computations of the theoretical flow response across a linear sand bank, followed by calculations of sediment transport rates associated with this flow response and taking into account the actual wave and current conditions in the study area. For this purpose the 1D hydrodynamic model *Trenchflow* (Boer, 1985) was used in combination with the 2DV morphodynamic model *Sutrench* (Van Rijn, 1986).

The use of these models in a complicated three-dimensional area is justified for the present purpose, as the objective of the modelling exercise is to obtain a first-order sensitivity analysis of the relevant processes. The analysis is done for a cross-section in the middle part of a sand bank, where the interaction between water motion and morphology is considered a local phenomenon. The applied models can be used for this situation, as they are valid for ridges of infinite length. Consequently, the lateral coherence of linear sand bank systems (Fig. 1) is not considered in this paper, since it requires the aforementioned type of morphodynamic modelling which takes into account the dynamic behaviour of the entire morphodynamic system (e.g. Hulscher, 1996).

2. Model description

2.1. Hydrodynamic model — theoretical flow pattern across a linear sand bank

Assuming stationary flow conditions ($\partial/\partial t = 0$) and neglecting the Coriolis force and the turbulent shear stresses, the vorticity equation given by e.g. Abraham et al. (1987) can be rewritten as

$$u\frac{\partial \omega}{\partial x} + v\frac{\partial \omega}{\partial y} = \frac{\omega}{h}\left(u\frac{\partial h}{\partial x} + v\frac{\partial h}{\partial y}\right) + u\frac{\partial r}{\partial y} - v\frac{\partial r}{\partial x} - r\omega, \tag{1}$$

where x, y are the horizontal coordinates (m), u, v are the depth-averaged velocity components in x and y directions (m/s), h is the water depth (m), r the bottom shear stress factor ($= g|U|/C^2h\,(\mathrm{s}^{-1})$), $|U|$ the magnitude velocity vector (m/s), g the gravitational acceleration (m/s^2), C the Chezy constant ($= 18\log(12h/k_s)$), k_s the effective bed roughness (m), and ω the vorticity of the depth-averaged velocity field ($= \delta v/\delta x - \delta u/\delta y\,(\mathrm{s}^{-1})$).

Assuming uniformity in the crest direction and choosing the coordinate system given in Fig. 2 (y is directed parallel to the bank crest), all terms with $\partial/\partial y$ can be neglected. As a result, Eq. (1) reduces to

$$u\frac{\mathrm{d}\omega}{\mathrm{d}x} = \frac{\omega}{h}u\frac{\mathrm{d}h}{\mathrm{d}x} - \frac{\mathrm{d}r}{\mathrm{d}x} - r\omega. \tag{2}$$

With the same assumptions, the continuity equation reads

$$\frac{\partial}{\partial x}(hu) = 0. \tag{3}$$

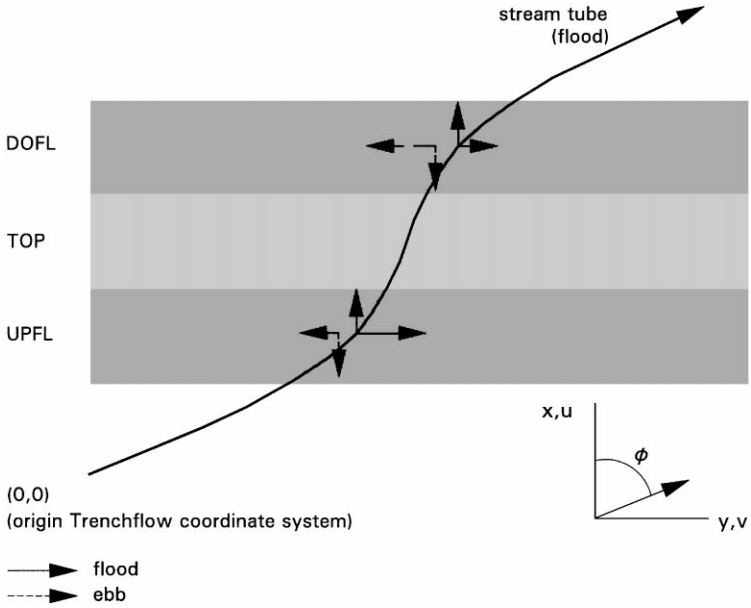

Fig. 2. Coordinate system *Trenchflow* (after Boer, 1985). UPFL = up-current flank; TOP = top of the ridge; and DOFL = down-current flank.

The assumption of stationary flow conditions ($\partial/\partial t = 0$) is an important one, since it neglects a number of non-linear interactions (see e.g. Hulscher, 1996). However, as a first-order approximation this is considered reasonable, especially when taking into account that most, if not almost all, sediment transport takes place during maximum flow conditions.

The assumption of lateral continuity implies that at least locally the current is dominated by its interaction with the ridge topography. Although observations suggest the opposite, the modelling still presents the expected first-order maintenance process by friction-induced veering of oblique flows towards the ridge crest, the basic flow response in the models of Huthnance (1982) and De Vriend (1990).

Eqs. (2) and (3) have been solved numerically by Boer (1985) and incorporated into a mathematical model (*Trenchflow*). This model computes the current velocity along the streamlines across the sand bank (or any other infinitely long positive or negative topographic feature). The required input parameters for the model are the sand bank wavelength (L), sand bank height (h_{bank}), the undisturbed depth-averaged current velocity magnitude (U_0) and current direction with respect to the bank axis (φ_0), the undisturbed water depth (h_0) and the bottom roughness (k_{s}).

2.2. Sediment transport and bed evolution

When a current passes a sand bank, the flow velocity and hence the sediment transport capacity increases and sediment particles will be eroded from the bank.

A simulation of sedimentation and erosion can be obtained from a detailed mathematical approach, modelling all relevant phenomena such as the increased turbulence generated by the decelerated flow, the current- and wave-related mixing processes and the intensified pick-up of bed material by the accelerated flow. These processes are simulated by the two-dimensional vertical mathematical model *Sutrench* (Van Rijn, 1986, 1993, 1998), which is valid for flows (plus waves) across ridges of infinite length.

2.2.1. Basic equation for sediment concentrations

The computation of the concentrations is based on a numerical solution of the convection–diffusion equation. Assuming steady-state conditions and neglecting the transport by longitudinal mixing, which is relatively small, the convection–diffusion equation can be expressed as

$$\frac{\partial}{\partial x}(buc) + \frac{\partial}{\partial z}[b(w - w_s)c] - \frac{\partial}{\partial z}\left(b\varepsilon_{s,cw}\frac{\partial c}{\partial z}\right) = 0, \tag{4}$$

where u is the longitudinal velocity at height z above the bed (m/s), c the sediment concentration (kg/m^3), w the vertical flow velocity (m/s), w_s the particle fall velocity of suspended sediment (m/s), $\varepsilon_{s,cw}$ the sediment mixing coefficient by current and waves (−), b the flow width (m), x longitudinal coordinate (m), and z the vertical coordinate.

The flow width (b) is introduced to represent the sediment transport in a gradually diverging or converging flow. The flow velocities and sediment concentrations are assumed to be constant in lateral direction. Using this approach, the transport processes in a stream tube refracted on a sand bank oblique to the approaching current can be represented. The flow width as a function of distance ($b(x)$) must be known a priori (field survey, physical-scale model or mathematical model) and specified to the *Sutrench* model. For the present case the results of the *Trenchflow* model were used. Eq. (4) can be solved numerically, when the flow velocities, the sediment mixing coefficients and the particle fall velocity are known.

2.2.2. Velocity profiles in gradually varying flows

The flow velocity profiles in a gradually varying flow are assumed to be logarithmic:

$$u = \frac{u_k}{\ln(h/z_0)}\ln(z/z_0), \tag{5}$$

$$u_h = \frac{\ln(h/z_0)}{-1 + \ln(h/z_0)}\frac{Q}{bh}, \tag{6}$$

where u is the longitudinal flow velocity (m/s), u_h the water surface velocity (m/s), h the water depth (m), Q the discharge (m^3/s), z the height above bed (m), z_0 the zero-velocity level (0.033 k_s) (m), and k_s the effective bed roughness height (m).

The effect of the waves on the velocity distribution is neglected. The vertical flow velocity (w) can be computed from the fluid continuity equation as follows:

$$w = -\int_{z_0}^{z}\frac{\partial u}{\partial x}\,\mathrm{d}z - \frac{1}{b}\frac{\mathrm{d}b}{\mathrm{d}x}\int_{z_0}^{z} u\,\mathrm{d}z \tag{7}$$

yielding a rather simple analytic expression. The bed-shear velocity (u_*) follows from

$$\frac{u_h}{\ln(h/z_0)} = \frac{u_*}{\kappa}. \tag{8}$$

Eq. (8) can be expressed as

$$u_* = \frac{\kappa}{-1 + \ln(h/z_0)} \frac{Q}{bh}, \tag{9}$$

where κ is the constant of Von Kármán.

2.2.3. Mixing coefficients for gradually varying flows with waves

The mixing coefficient is represented by a combination of the current-related and the wave-related mixing coefficient, as follows:

$$(\varepsilon_{s,cw})^2 = (\varepsilon_{s,c})^2 + (\varepsilon_{s,w})^2, \tag{10}$$

where $\varepsilon_{s,c}$ is the current-related sediment mixing coefficient and $\varepsilon_{s,w}$ the wave-related mixing coefficient.

The current-related mixing coefficient is described by

$$\varepsilon_{s,c} = \varepsilon_{s,c,max} - \varepsilon_{s,c,max}\left(1 \frac{2z}{h}\right)^2 \quad \text{for } \frac{z}{h} < 0.5, \tag{11a}$$

$$\varepsilon_{s,c} = \varepsilon_{s,c,max} = 0.25\beta\kappa u_{*,c} h \quad \text{for } \frac{z}{h} \geqslant 0.5, \tag{11b}$$

where $u_{*,c}$ is the current-related bed-shear velocity according to Eq. (9) and, β the ratio of sediment and fluid mixing coefficient (Van Rijn, 1986, 1993).

The wave-related mixing coefficient is described by

$$\varepsilon_{s,w} = \varepsilon_{s,w,bed} \quad \text{for } z \leqslant \delta, \tag{12a}$$

$$\varepsilon_{s,w} = \varepsilon_{s,w,max} \quad \text{for } z \geqslant 0.5h, \tag{12b}$$

$$\varepsilon_{s,w} = \varepsilon_{s,w,bed} + (\varepsilon_{s,w,bed})\left(\frac{z-\delta}{0.5h-\delta}\right), \tag{12c}$$

where $\varepsilon_{s,w,bed}$ is the wave-related mixing coefficient close to the bed, $\varepsilon_{s,w,max}$ the wave-related mixing coefficient in the upper half of the water depth, and δ the thickness of near-bed mixing layer (Van Rijn, 1986, 1993).

Eq. 12 is based on the analysis of measured concentration profiles for waves alone. The characteristic parameters of the mixing coefficient distribution were related to general wave parameters, yielding

$$\varepsilon_{s,w,bed} = \alpha_1 \delta \cap \hat{u}_{b,w}, \tag{13}$$

$$\varepsilon_{s,w,max} = \alpha_2 \frac{hH_s}{T_s}, \tag{14}$$

where H_s is the significant wave height, $\hat{u}_{b,w}$ the peak value of near-bed orbital velocity according to linear wave theory, T_s the significant wave period, α_1 a coefficient $(= 0.0006D_*^2)$, α_2 a coefficient $(= 0.035)$, D_* the particle parameter $(= D_{50}(1\,g/v^2)^{1/3})$, $\Delta(= (\rho_s - \rho)/\rho, \rho_s$ the sediment density, ρ the fluid density, g the acceleration due to gravity, and v the kinematic viscosity coefficient (Van Rijn, 1993, 1998).

2.2.4. Boundary conditions

The following specifications are required:

Flow domain:	initial bed levels, water depth, flow width, wave characteristics, particle fall velocity, effective bed roughness, size, composition and porosity of bed material;
Inlet boundary:	discharge, flow velocities, mixing coefficients, concentrations;
Water surface:	net vertical transport is assumed to be zero;
Bed surface:	bed concentration of upward sediment flux at bed as a function of local flow and sediment parameters.

The bed-boundary condition is specified at a small height $(z = a)$ above the mean bed. Using this approach, the bed concentration or the sediment flux can be represented by its equilibrium values, assuming that there is an almost instantaneous adjustment to equilibrium conditions close to the bed.

For equilibrium conditions Van Rijn (1986, 1993) proposed the following bed-concentration function:

$$c_a = 0.015\,\frac{D_{50}}{a}\,\frac{T^{1.5}}{D_*^{0.3}}, \tag{15}$$

where c_a is the bed concentration, a the reference level above bed, T the bed-shear stress parameter $(= (\bar{\tau}_{b,cw} - \bar{\tau}_{b,cr})/\bar{\tau}_{b,cr})$, $\bar{\tau}_{b,cw}$ the effective bed-shear stress $(= \mu_c\bar{\tau}_{b,cr} + \mu_w\bar{\tau}_{b,w})$, $\bar{\tau}_{b,c}$ the current-related bed-shear stress, $\bar{\tau}_{b,w}$ the wave-related bed-shear stress according to linear wave theory, μ_c the current-related efficiency factor, μ_w the wave-related efficiency factor $(= 0.8/D_*)$, and $\bar{\tau}_{b,cr}$ the critical bed-shear stress according to Shields.

2.2.5. Bed-level computation

Bed-level changes are computed from the cross-section integrated sediment continuity equation, which reads

$$\frac{\partial}{\partial t}\,(bz_b) + \frac{1}{\rho_s(1-p)}\,\frac{\partial}{\partial x}\,(S_s + S_b) = 0, \tag{16}$$

where t is the time, b the flow width, z_b the bed-level above a horizontal datum, p the porosity factor, S_s the suspended load and S_b the bed load.

The suspended load is computed as

$$S_s = b\int_a^h uc\,\mathrm{d}z. \tag{17}$$

The bed-load transport is described by the following formula (Van Rijn, 1993):

$$S_b = 0.053b(\Delta g)^{0.5} D_{50}^{1.5} \frac{T^{2.1}}{D_*^{0.3}}. \quad (18)$$

2.2.6. Numerical solution methods

To solve Eq. (4), a finite-element method is used. The continuous solution domain is divided into a system of quadrangular elements. The vertical dimensions of the elements decrease towards the bed to provide a greater resolution in the zone where large velocity and concentration gradients exist. To solve Eq. (16), a conservative LAX scheme is used.

2.2.7. Calibration of the Sutrench model

Sediment transport calculations obtained with the morphodynamic model *Sutrench* were compared to the fair-weather in situ measurements presented in Part 1 of this paper (see also Van de Meene and Van Rijn, 1994). Comparison of the observed bed load and suspended load transport rates with those calculated by the *Sutrench* model shows that this model fails to predict the sediment transport rates at low current velocities correctly (Van de Meene and Van Rijn, 1994). At higher current velocities, the bed load sediment transport rates are predicted reasonably well, while the suspended load transport rate is over predicted by a factor 4. The limited agreement is attributed to the uncertainty of the bed roughness k_s. This parameter is difficult to measure in the field accurately, while it has a large effect on the computed sediment transport rates.

Especially during fair-weather conditions, k_s may vary between grain roughness and ripple roughness. Van de Meene and Van Rijn (1994) used a k_s value of 0.05 m. The limited amount of field observations at low transport rates therefore are not representative to test sediment transport models. A large number of measurements, with careful sampling along all parts of the bed topography (stoss side, lee side, crest and trough of the ripple field) are required to obtain a more representative data set (see Van Rijn and Gaweesh, 1992 for river conditions). Unfortunately, however, such measurements are hardly feasible in the marine environment.

A detailed discussion on the determination of k_s in the field in relation to small-scale bed forms is beyond the scope of this paper. The sensitivity of the sediment transport calculations to k_s, however, indicates that this sensitivity should be taken into account in the *Sutrench* model calculations presented in this paper.

Time-averaged suspended sediment concentrations, measured during storm conditions were compared with computed sediment concentrations based on the *Sutrench* model. The results are given in Fig. 3. Although there is considerable scatter, most calculated concentrations correspond within a factor 2, which is considered reasonable. The comparison between observations and theory gives better results than in the fair-weather case. This is attributed to the fact that the model is better calibrated for high-energy conditions with plane bed or washed out ripples than for low-energy conditions with ripples close to initiation of motion. In this latter regime, horizontal variations of concentrations related to ripple

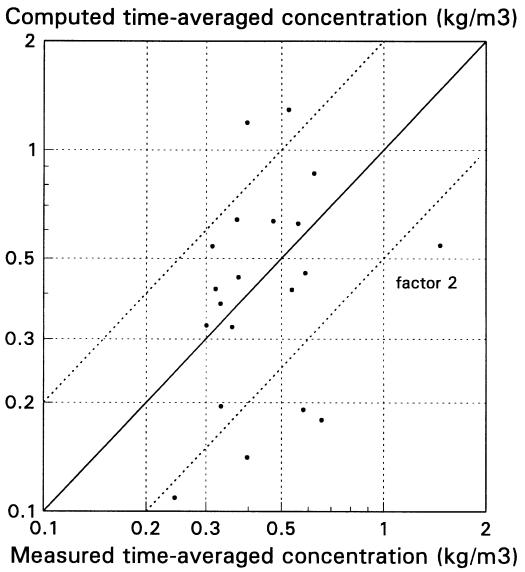

Fig. 3. Comparison between observed and computed near-bed sediment concentrations during a storm.

geometry are relatively large. Sedimentological observations indeed have shown that the sea bed may become almost flat during such storm conditions (Van de Meene et al., 1996). Possible explanations for the observed scatter are variations in measurement height and bed topography.

3. Morphological evolution of a sand bank

3.1. Introduction

The combination of the *Trenchflow* and *Sutrench* models described in the previous section gives a simple morphodynamic model which allows for a preliminary study of the morphological evolution of a sand ridge of infinite length. For the sand ridges in the study area an initial sedimentation/erosion (ISE) model was employed, i.e. the bottom topography was assumed to be invariant (De Vriend et al., 1993). The basis for this was that the morphological time scale was considered to be much larger than the tidal time scale (tidal period). The results revealed that this assumption was justified (morphological time scale order hundreds or thousands of years).

The characteristic response of the tidal flow across a ridge was studied with the *Trenchflow* model, applying Eqs. (2) and (3) from the previous section. The calculated flow response was subsequently used as input for the *Sutrench* model. This model allows for a calculation of the sediment transport pattern across the sand ridge and its subsequent morphological evolution. Since an initial morphodynamic model was considered, morphological changes were calculated from the sediment budgets for each morphological unit of the sand ridge (up-current flank, top and

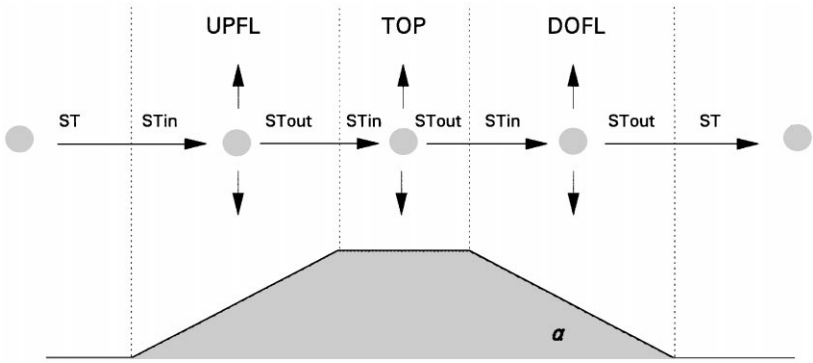

Fig. 4. Definition of the sand bank topography used for the *Sutrench* calculations: UPFL = up-current flank; TOP = top of the ridge; DOFL = down-current flank; and ST = total sediment transport.

down-current flank, Fig. 4). Both *Trenchflow* and *Sutrench* calculations were supplemented with a sensitivity analysis.

3.2. Flow characteristics: an example

The flow response for conditions characteristic for the study area (flood spring tidal current velocity $U_0 = 0.8\,\mathrm{m/s^{-1}}$ and direction $\varphi_0 = 75°$; sand bank wavelength $L = 2500\,\mathrm{m}$; sand bank height $h_{\mathrm{bank}} = 4\,\mathrm{m}$; $h_0 = 18\,\mathrm{m}$, $k_s = 0.05\,\mathrm{m}$) is given in Fig. 5. The acceleration of the cross-bank component at the bank crest follows directly from the continuity equation (Eq. (3)), the deceleration of the along-bank component is caused by the increased bottom friction at the bank crest.

These velocity variations cause the current to veer towards the crest. Since the along-bank velocity (v) is larger than the cross-bank velocity (u), the total velocity magnitude decreases at the ridge crest. Fig. 5 shows a phase shift of the along-bank and total velocity variation with respect to the bottom topography, caused by the inertia effect. Fig. 5 also shows that the along-bank velocity component at the up-current flank of the ridge is always stronger than that at the down-current flank. Averaged over a tidal cycle, this gives the residual circulation around the sand bank, as discussed by e.g. Zimmerman (1981).

The effect of the bank height (h_{bank}) on the flow response was analysed by considering four different bank heights (Fig. 6(a) and Table 1). For bank heights between 2 and 8 m (h_{bank}/h_0 between 0.11 and 0.44), the nature of the flow response was the same, while the magnitude of the velocity perturbations varied. The maximum velocity difference between the up- and down-current flank varied between 4 and 17%. For a bank height of 4 m ($h_{\mathrm{bank}}/h_0 = 0.22$), the velocity perturbation amounted to 8% (Figs. 5 and 6(a)). The expected tide-averaged residual circulation around the ridges is approximately equal to the magnitude of the velocity perturbation.

The sand bank orientation affects the nature of the response, which is evident when two extreme cases are considered: flow almost perpendicular to the sand bank ($\varphi_0 = 5°$) and flow almost parallel to the sand bank ($\varphi_0 = 85°$; Fig. 6(b)). In the first

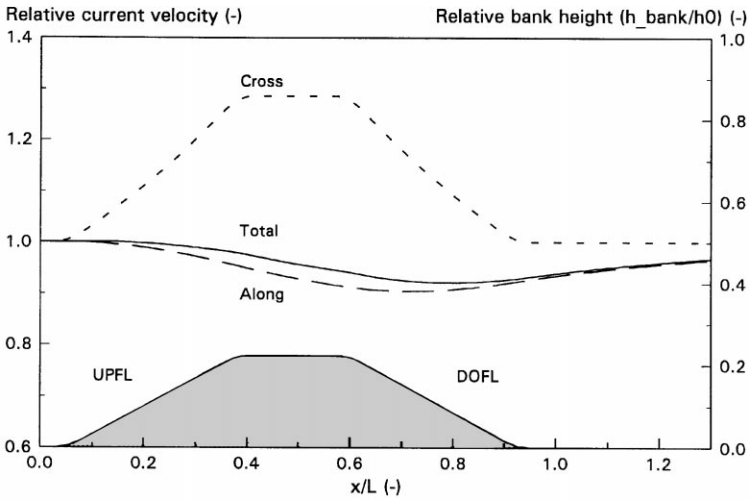

Fig. 5. Flow response across a linear sand bank. Reference conditions typical for a spring tidal flood current ($U_0 = 0.8\,\mathrm{m/s}$, $\phi_0 = 75^\circ$, $L = 2500\,\mathrm{m}$, $h_{\mathrm{bank}} = 4\,\mathrm{m}$, $h_0 = 18\,\mathrm{m}$, $k_s = 0.05\,\mathrm{m}$; UPFL = up-current flank, DOFL = down-current flank).

case there is no net decrease of the total current velocity, since continuity is the only effect at work in this situation. For almost parallel flow, the velocity decrease is at its maximum, but since the current flows almost parallel to the bank, this deceleration is not advected over the crest. There is thus an optimum velocity variation for maintenance of the sand bank at intermediate angles φ.

Eq. (2) has an inertial part and a friction part (Boer, 1985). Inertia is dominant with relatively steep slopes and thus short wavelengths. As a result, there is no flow deceleration and sedimentation for short bank lengths and therefore no maintenance of the sand bank (Fig. 6(c)). In intermediate conditions both inertia and friction play a role. With the model characteristics given before, the flow appears to be inertia-dominated for a wavelength of 250 m, while both inertia and friction are important for wavelengths of 2500 m.

The effective bed roughness (k_s) also affects the flow response across a sand bank. The general trend is that the flow response will be larger and occur earlier (shorter lag) when the bed is rougher (k_s is larger), and vice versa. In practice however, this effect is very small. Taking $k_s = 0.05\,\mathrm{m}$ as a reference condition, velocities for $k_s = 0.01\,\mathrm{m}$ differ by at most 2%, while velocities for $k_s = 0.10\,\mathrm{m}$ vary with a maximum of 1%.

3.3. Sediment transport: examples

The sediment transport pattern across a linear sand bank was based on the flow response of Fig. 5. Although there is only partial correspondence between nature and theory, these calculations provide a first-order idea of the behaviour of the ridge

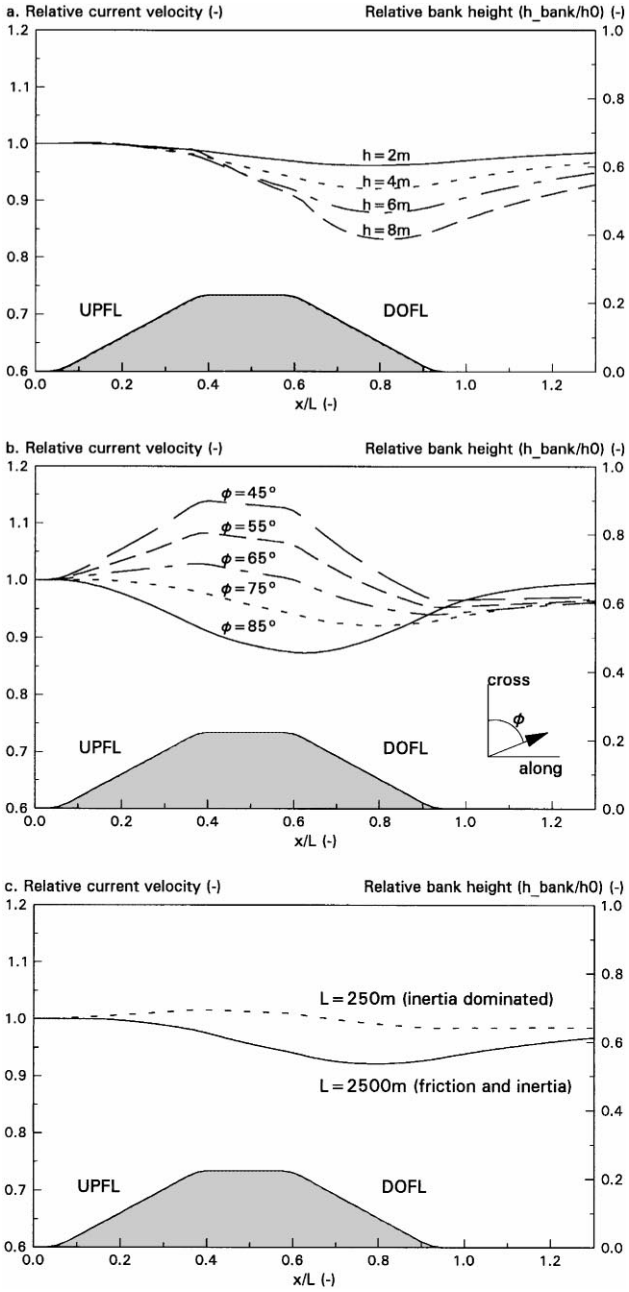

Fig. 6. Sensitivity analysis *Trenchflow*. Reference conditions as in Fig. 5. (a) Flow response (total velocity vector) as a function of sand bank height h_{bank}; (b) flow response as a function of sand bank orientation with respect to the undisturbed flow ϕ_0; and (c) flow response as a function of sand bank wavelength L. Summary of input conditions given in Table 1.

Table 1
Input conditions sensitivity analysis *Trenchflow*[a]

	Run	$\|U_0\|$ (m/s)	ϕ_0 (deg)	L (m)	h_{bank} (m)	h_0 (m)	k_s (m)
Fig. 6(a)	3	0.8	75	2500	2	18	0.05
	4	0.8	75	2500	4	18	0.05
	5	0.8	75	2500	6	18	0.05
	6	0.8	75	2500	8	18	0.05
Fig. 6(b)	7	0.8	85	2500	4	18	0.05
	8	0.8	75	2500	4	18	0.05
	9	0.8	65	2500	4	18	0.05
	10	0.8	55	2500	4	18	0.05
	11	0.8	45	2500	4	18	0.05
Fig. 6(c)	1	0.8	75	2500	4	18	0.05
	2	0.8	75	250	4	18	0.05
Not shown	12	0.8	75	2500	4	18	0.01
	13	0.8	75	2500	4	18	0.05
	14	0.8	75	2500	4	18	0.10

[a] U_0 = undisturbed current velocity (magnitude); ϕ_0 = undisturbed current velocity (direction); L = wavelength of the bank; h_{bank} = height of the bank; h_0 = undisturbed water depth; and k_s = bed roughness.

system in the present hydrodynamic regime. In addition, similar calculations were done using the observed flow response as input.

The most important input parameters for the sediment transport calculations with the *Sutrench* model are (also see Section 2.2): bottom profile; stream tube width; time-dependent wave data and current velocity across the ridge. The current velocities from the *Trenchflow* computations were implemented in the *Sutrench* model by varying the stream tube width (b) along the bottom profile, taking $b = 1$ at $x = 0$ (Fig. 5). The current velocities in the *Sutrench* model follow from $u = Q/bh$, with Q the discharge (m^3/s), h the local water depth (m), and b the local stream tube width (m).

Typical spring and neap tidal current velocities in the study area are given in Fig. 7. Based on these curves, the tidal currents were kept constant during each tidal phase, with an effective flood current of 0.7 m/s and an effective ebb current of 0.6 m/s (Table 2), each with an effective duration of 3 h per tidal cycle. The effect of wind-driven flow was not considered because of lack of input data. A summary of input conditions is given in Table 2.

Computed sediment transport rates by a tidal current alone (flood velocity, no waves) and by this current combined with extreme storm waves ($H_s = 5$ m, $T_p = 9$ s) are given in Figs. 8(a) and (b). The sediment transport rates increase at the up-current flank and decrease at the ridge crest and at the down-current flank. There is thus erosion at the up-current flank and sedimentation at the top and down-current flank, for both conditions. The relative decrease in sediment transport rate (i.e. $(S_{UPFL} - S_{DOFL})/S_{UPFL}$), and thus the relative sedimentation rate, is largest in the case without waves (Fig. 8(a); especially at the top of the bank). This is due to the

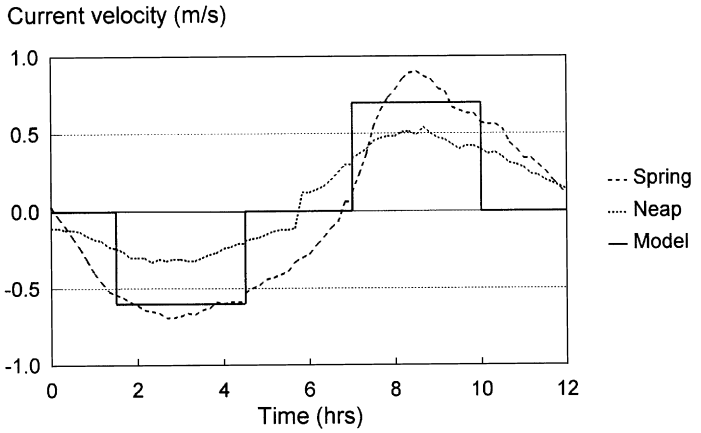

Fig. 7. Characteristic tidal velocity curve and schematized velocity regime. Positive is flood; negative is ebb.

Table 2
Summary of the input conditions for the *Sutrench* model runs[a]

Tidal currents		Wave conditions		Water level		Bank height	Bed roughness
Phase	U_0 (m/s)	H_s (m)	T_p (s)	$h_{0,flood}$ (m)	$h_{0,ebb}$ (m)	h_{bank} (m)	k_s (m)
Flood	0.7	0	—	18	18	2	0.01
Ebb	0.6	1	6	18	16	4	0.05
		2	6			6	0.10
		3	7			8	
		4	8				
		5	9				

[a] Phase = tidal phase (ebb/flood); U_0 = undisturbed current velocity magnitude; H_s = significant wave height; T_p = peak wave period; $h_{0,flood}$ = undisturbed water depth during flood; $h_{0,ebb}$ = undisturbed water depth during ebb; h_{bank} = height of the bank; and k_s = bed roughness.

fact that during fair-weather conditions the sediment transport is dominated by bed load, which adapts faster to variations in hydraulic conditions across the ridge than the suspended load transport during storms. The settling of suspended sediment is a relatively slow process. Comparison of Figs. 5 and 8 shows that there is erosion at the up-current flank, despite the small decrease in current velocity. This is due to the increase of the bed friction (decrease of water depth) and associated increase in bed shear stress and hence sand transport rate. Apparently, the effect of the decreasing depth at the up-current flank compensates for the local small decrease in current velocity.

The effect of the bed roughness (k_s) on the sediment transport rates (especially the suspended transport) was studied by varying k_s between 0.01 and 0.10 m, keeping $k_s = 0.05$ m as a reference condition. Results are given in Figs. 8(a) and (b) as well. Sediment transport rates are more sensitive to variations in k_s for large waves than for smaller or no waves. For $k_s = 0.01$ m, mean sediment transport rates through

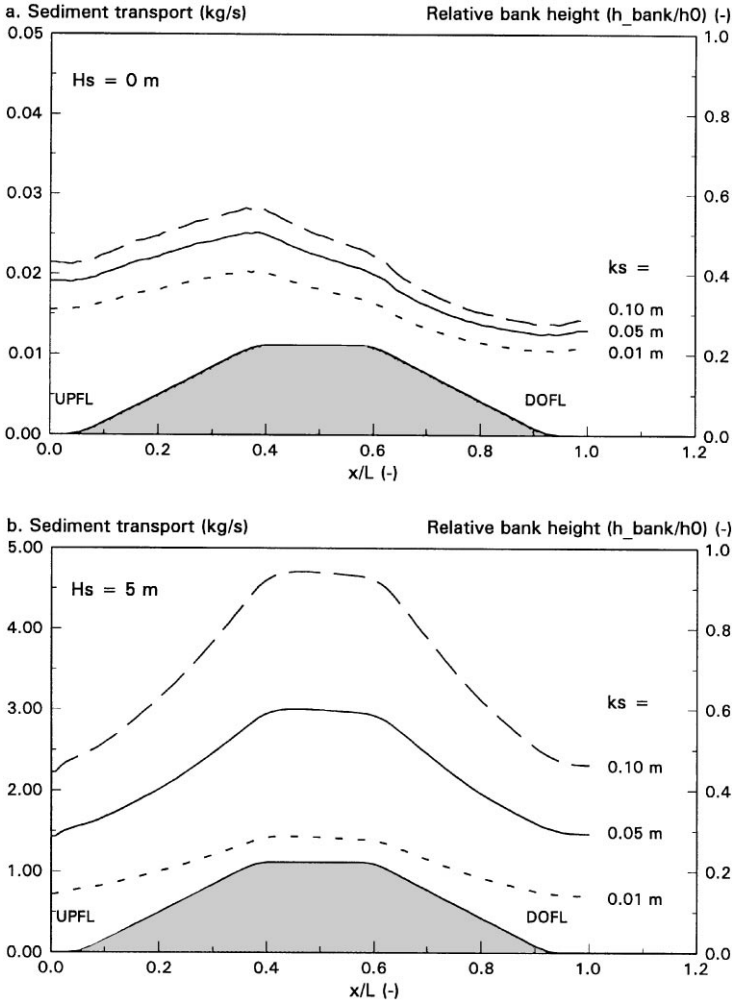

Fig. 8. Sediment transport rates across a linear sand bank calculated with *Sutrench*. Input is the flow response given in Fig. 5 (reference conditions for a typical spring tidal flood current). UPFL = up-current flank, DOFL = down-current flank. (a) $H_s = 0$ m, $k_s = 0.01$, 0.05, 0.10 m; (b) $H_s = 5$ m, $k_s = 0.01$, 0.05, 0.10 m.

the morphological units of Figs. 8(a) and (b) were a factor 0.5 ($H_s = 5$ m) to 0.8 ($H_s = 0$ m) smaller than for $k_s = 0.05$ m. For $k_s = 0.10$ m, mean sediment transport rates were a factor 1.1 ($H_s = 0$ m) to 1.6 ($H_s = 5$ m) larger than for $k_s = 0.05$ m. These variations in sediment transport rates generally do not affect the nature of the morphological development, only the rate at which this development takes place.

Fig. 8 only shows sediment transport rates during the flood phase. Under a full tidal cycle, the sediment will be swept to and fro from one side of the sand bank to the other. Sedimentation at the ridge crest is predicted under both fair-weather and

storm conditions. This indicates that the considered sand bank system has a potential to grow, and to migrate if the tide is asymmetrical. No erosion at the ridge crest was observed under the considered conditions, even not during high waves. This means that the suggestion of Huthnance (1982) that storm waves may provide a mechanism balancing growth under quieter conditions does not apply for the situations considered here.

Fig. 9 gives the yearly flood 9(a), ebb 9(b) and tide-averaged 9(c) sediment transport rates across the studied sand bank for each individual wave class. The contribution of each wave class averaged over a year (i.e. sediment transport rate multiplied by the frequency of occurrence) is of the same order of magnitude, despite the large effect of wave height on the sediment transport rates, as evident from Fig. 8. This means that there is no dominance of either fair-weather or extreme conditions on the yearly sediment transport rates. A comparable result for another part of the North Sea has been described by Soulsby (1987). This author concluded that the most important contributions to the long-term sediment transport are made by fairly large but not too infrequent waves, combined with tidal currents between mean neap and maximum spring tide. Weak currents and low waves give a small contribution, because their potential for sediment transport is low, although their frequency is high. Extreme conditions also are relatively unimportant, since, although their transport potential is high, their frequency is too low.

The tide-averaged sediment transport rates are dominated by average conditions ($H_s = 1$ m, Fig. 9(c)), while the contribution of high waves is smaller than for the instantaneous flood and ebb sediment transport rates (Figs. 9(a) and (b)). Apparently, the tide-averaged effect of higher wave conditions is almost zero. This may be explained by the balancing effects of water level and current velocity variations. During flood, current velocities and water depth are higher than during ebb. Due to the larger water depths during flood, the effect of the waves on the sediment transport rates is smaller. The result for high wave conditions, as evident from Fig. 9, is that stronger current velocities with weaker wave effects during flood are balanced by weaker currents with stronger wave effects during ebb. The overall result is that the net effects are mainly determined by non-extreme waves between 0 and 2 m.

The total yearly sediment transport rates over the ridges vary between approximately 115 and 160 $m^3/m\,yr$ for the flood phase and between 75 and 125 $m^3/m\,yr$ for the ebb phase (minimum in the upstream trough and maximum at the ridge crest, see Fig. 8). Consequently, net sediment transport rates across the ridges are around 35 $m^3/m\,yr$ in the direction of the dominant flood tidal current (roughly northwards). These values correspond well with the results of an extensive modelling study of the Dutch coast (Van Rijn, 1997). According to this study, net sediment transport rates in a coastal section a few kilometres south of the ridge area (Noordwijk) were $35 \pm 15\,m^3/m\,yr$ at the -20 m line and $85 \pm 45\,m^3/m\,yr$ at the -8 m line.

3.4. Sand bank evolution

The morphological evolution of a linear sand bank, i.e. its growth and migration rate and its dependence on current velocity, wave height, water depth and bank

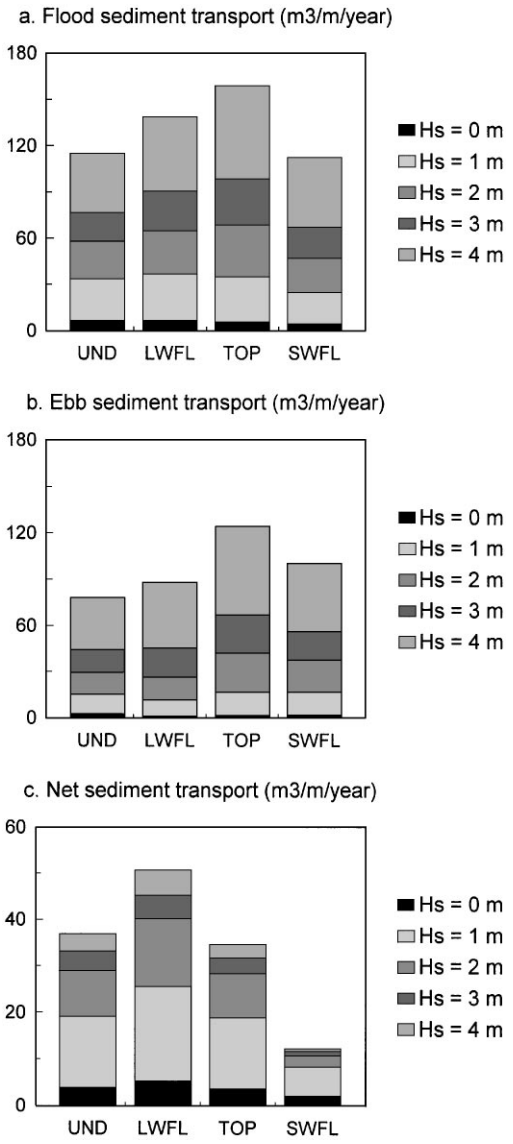

Fig. 9. Yearly sediment transport rates across a linear sand bank weighted for the wave climate. UND = undisturbed (flat) sea bed, LWFL = landward flank (up-current flank during flood, down-current flank during ebb, Fig. 1), SWFL = seaward flank (down-current flank during flood, up-current flank during ebb, Fig. 1). (a) Flood transport ($U_0 = 0.7$ m/s, $h_0 = 18$ m); (b) ebb transport ($U_0 = 0.6$ m/s, $h_0 = 16$ m); (c) residual transport (flood minus ebb). All other input conditions as in Fig. 5.

height was studied by analysing the sediment balance for the different morphological units of the bank, as depicted in Fig. 4. The sediment balance for this sand bank system reads

$$\Delta z = \frac{G}{\rho_s(1-\varepsilon)\overline{\overline{BL}}} \tag{19}$$

with

$$G = (ST_{in} - ST_{out})T \tag{20}$$

in which Δz is the bed-level change (m), G the weight of the sediment deposited during time T (kg), ρ_s the density of the sediment (kg/m), ε the porosity (−), $\overline{B}$ the mean width of the stream tube (m), $\overline{L}$ the mean length of the stream tube (m), ST_{in} the total sediment transport load through the stream tube into the morphological unit (kg/s), ST_{out} the total sediment transport load through the stream tube out of the morphological unit (kg/s), and T the time (s).

The velocity response and the mean stream tube width and length, as calculated with the *Trenchflow* model, provides the input for the *Sutrench* model. This latter model gives the total sediment transport into and out of each morphological unit depicted in Fig. 4. The calculations were done for conditions characteristic for the study area (Table 2). The tidal current velocities used as input were based on measurements near the ridges, while the wave climate was obtained from a nearby measurement station (Meetpost Noordwijk; Roskam, 1988). The effect of tidal water-level variations was studied by considering two extremes: no water-level variations and a typical spring tidal range of 2 m. Furthermore, the morphological behaviour of the sand bank was analysed for different bank heights.

The general trends in morphological evolution are erosion of the up-current flank and deposition at the top and on the down-current flank. Both migration rates and deposition at the top increase for increasing bank height. For a sand bank of 4 m high, tide- and wave climate-averaged bed-level changes are in the order of 0.010–0.015 m/yr.

The vertical bed-level changes Δz at the up- and down-current flank may be converted into horizontal migration rates Δx, using simple geometrical rules: $\Delta x = \Delta z/\tan\alpha$, in which α is the slope of the flank. The slope of the considered sand bank (Fig. 4) is about 1 : 210. This gives estimated horizontal migration rates for the 4 m bank ranging between 1 and 3 m/yr in the direction of the flood current, for maximum water-level variations (18/16 case, Table 2) and no water-level variations (18/18 case), respectively. This corresponds to a migration in the order of a sand bank wavelength in a few thousands of years. A geological reconstruction of the sand banks in the study area has revealed a similar migration rate (Van de Meene, 1994). There is thus a good correspondence between the model calculations and this geological reconstruction. The calculated vertical aggradation rates at the top are relatively large, 0.015 m/yr (or 1.5 m/century) for the 4 m bank. This aggradation rate increases with increasing bank height. This indicates a positive feedback: in the present model, the initial sand bank is predicted to grow, while there is no damping, even not during high-wave conditions.

There is a marked effect of the water-level variations on the sand bank behaviour. When water-level differences between ebb and flood are ignored (water depth is 18 m during both ebb and flood), the dominant flood current dictates the migration direction (erosion at the landward flank, sedimentation at the seaward flank). When water-level variations are taken into account (water depth is 18 m during flood and 16 m during ebb), the ebb transport dominates the flood transport during high waves, due to the lower water-levels during ebb. As a result, the flood-dominance observed in the 18/18 case is reduced in the 18/16 case for the 2 and 4 m banks. This results in lower flood-dominated migration rates. The 6 and 8 m banks are predicted to migrate with the ebb-current. The sedimentation at the top is not affected by the water-level variations.

Since sand bank growth is predicted for all input conditions studied here, the question arises which mechanism may balance this growth. Van de Meene and Van Rijn (2000) have shown that the theoretical flow response used for the present model calculations (Fig. 5) is not observed in nature, at least not with the same velocity variations. This natural situation was simulated by calculating the morphological evolution of the sand bank under a tidal current crossing the sand bank obliquely, with no variation in current velocity or direction across the sand bank (i.e. observed flow conditions). The migration rates for these real flow conditions are generally comparable to those based on the theoretical flow conditions. However, the relatively large sedimentation rates at the top under theoretical flow conditions have changed into small erosion rates at the top (order 0.002 m/yr) during observed flow conditions. The absence of the theoretical flow response thus may form an erosion mechanism balancing sand bank growth.

The cross-sectional area of the sand bank depicted in Fig. 4 is approximately 5000 m^2. The mean stream tube width in the *Sutrench* calculations varies between 1 and 1.6 m. This means that the volume of the sand bank per stream tube width is in the order of 5000–8000 m^3. The net sediment transport gradient through the stream tube for all wave and tide classes amounts to 33 m^3/yr, which is much less (order factor 200) than the total volume of sand stored in the ridges. Therefore, no major morphological changes in the sand banks are expected on the time scale of years. However, on the geological time scale of, say, 1000 yr, the total amount of eroded and deposited sediment is larger than the volume of sediment stored in the ridges (order factor 5). This indicates that the sand banks are probably not a relict on this geological time scale.

4. Discussion and conclusions

The model calculations have shown that the ridges have a potential to grow and to migrate under the theoretical flow regime. The net sediment transport gradients through a stream tube over a period of a year are much smaller than the volume of the sandbank under the stream tube, indicating that the ridges are stable over a period of years to decades. On a time scale of thousands of years, sediment reworking is larger than the volume stored in the ridges. This suggests that the ridges were formed or at least maintained in the present hydrodynamic regime and that

they are not a geological relict. This outcome is supported by a geological reconstruction of the formation of the ridges (Van de Meene, 1994). The above results also indicate that the morphological time scale of the ridges is in the order of hundreds or thousands of years, which justifies the application of a local ISE model as a tool for process analysis.

By considering several extreme situations, the calculations provide a range of growth and migration rates for the considered sand bank system. Growth rates depend on the intensity of the flow response and are between + 0.015 and − 0.002 m/yr. Calculations based on the flow observations in nature suggest that the actual growth rate is close to zero.

Migration rates depend on the intensity of the flow response and on the magnitude of the water-level variations. The calculated migration rates are between 0.7 m/yr in ebb direction and 3 m/yr in flood direction. Calculations based on the observed flow conditions suggest that the actual migration rate is in the order of 0.5–1 m/yr in the direction of the dominant flood tidal current. This migration rate corresponds well with the results of a geological reconstruction (Van de Meene, 1994).

The *Sutrench* calculations have shown that, with the present ridge height, storm waves are not likely to flatten the ridges. Therefore, waves do not provide a mechanism balancing the predicted growth in the present situation. However, the *Sutrench* calculations have also shown that the observed flow response (i.e. veering but no velocity variation across the ridges) will cause a slight erosion, instead of growth. This suggests that a flow response weaker than the theoretical one may provide a situation in which the ridges are in equilibrium with the hydrodynamic regime.

In order to be able to draw firmer conclusions and to have a more rigorous validation of the mathematical model concepts discussed in Section 2 of Part 1 of this paper (Van de Meene and Van Rijn, 2000), the models should be adjusted to the actual situation, while the model results should be used to set up a further field measuring programme. In particular, the effect of wind- and density-driven currents on the bank morphology should be studied. However, the setting of the shoreface-connected ridges along the Dutch coast (the finite length of the ridges, the attachment to the shoreface and the proximity of the coastline) may be too complex to be described by a morphodynamic model like the ones mentioned before. This makes it difficult to assess what processes determine the formation and maintenance of these ridges. One way to overcome this problem is to perform 2D- or preferably 3D-model calculations with a realistic bottom topography and including the presence of the coastline. Such calculations are very time consuming, and therefore not suitable to study the morphodynamic evolution of the ridges (also see De Vriend et al., 1993). However, even their application to the actual morphological state may provide an impression of the sensitivity of the ridge system to the variability in hydrodynamic conditions (tidal currents, waves, wind- and density-driven effects), and of the effect of phenomena such as the finite length of the ridges, the attachment to the shoreface and the proximity of the coastline. The outcome of such model calculations should be compared with synoptic hydrodynamic measurements in the ridge area, to assess whether the predicted flow response can be observed in nature. Such synoptic observations may be obtained, for instance, with ship-borne acoustic

doppler current profilers (ADCPs), or with sets of stand-alone ADCPs deployed at the sea bed. The fact that this type of equipment has considerably improved technically over the last few years, while prices have gone down, should give a renewed boost into the field study of linear sand bodies.

Acknowledgements

This study was done within the framework of the Coastal Genesis Programme and was partly funded by the National Institute for Coastal and Marine Management (RIKZ) of the Ministry of Transport, Public Works and Water Management. We appreciate the useful comments of the reviewers on earlier versions of this paper.

References

Abraham, G., Gerritsen, H., Lindijer, G.J.H., 1987. Subgrid tidally induced residual circulations. Continental Shelf Research 7, 285–305.

Boer, S., 1985. The flow across trenches at oblique angle to the main flow direction. Delft Hydraulics, Report S 490, 39pp.

De Vriend, H.J., 1990. Morphological processes in shallow tidal seas. In: R.T. Cheng (Ed.), Coastal and Estuarine Studies, vol. 38: Residual Currents and Long–Term Transport, Springer, Berlin, pp. 276–301.

De Vriend, H.J., Zyserman, J., Nicholson, J., Roelvink, J.A., Péchon, P., Southgate, H.N., 1993. Medium-term 2DH coastal area modelling. Coastal Engineering 21, 193–224.

Hulscher, S.J.M.H., 1996. Formation and migration of large-scale, rhythmic sea-bed patterns: a stability approach. Ph.D. Thesis, Institute of Marine and Atmospheric Research, Utrecht University, 143pp.

Hulscher, S.J.M.H., De Swart, H.E., De Vriend, H.J., 1993. The generation of offshore tidal sand banks and sand waves. Continental Shelf Research 13, 1183–1204.

Huthnance, J.M., 1982. On one mechanism forming linear sand banks. Estuarine Coastal and Shelf Science 14, 79–99.

Roskam, A.P., 1988. Golfklimaten voor de Nederlandse kust. Rijkswaterstaat, Notitie GWAO-88.046 (in Dutch).

Soulsby, R.L., 1987. The relative contributions of waves and tidal currents to marine sediment transport. Hydraulics Research, Wallingford, Report No. SR 125, 11pp.

Van de Meene, J.W.H., 1994. The shoreface connected ridges along the central Dutch coast. Ph.D. Thesis, KNAG/Netherlands Geographical Studies 174, Utrecht, The Netherlands, 222pp.

Van de Meene, J.W.H., Van Rijn, L.C., 1994. Tide- and storm-driven sediment transport on the inner-shelf along the Dutch coast. Proceedings Coastal Dynamics '94. ASCE, New York, pp. 822–836.

Van de Meene, J.W.H., Boersma, J.R., Terwindt, J.H.J., 1996. Sedimentary structures of combined flow deposits from the shoreface-connected ridges along the central Dutch coast. Marine Geology 151–175.

Van de Meene, J.W.H., Van Rijn, L.C., 2000. The shoreface-connected ridges along the central Dutch coast — part 1: field observations. Continental Shelf Research 20, 2295–2323.

Van Rijn, L.C., 1986. Mathematical modelling of suspended sediment in non-uniform flows. Journal of Hydraulic Engineering 112, 433–455.

Van Rijn, L.C., 1993. Principles of Sediment Transport in Rivers, Estuaries and Coastal Seas. Aqua Publications, Amsterdam, The Netherlands.

Van Rijn, L.C., 1997. Sediment transport and budget of the central coastal zone of Holland. Coastal Engineering 32, 61–90.

Van Rijn, L.C., 1998. Principles of Coastal Morphology. Aqua Publications, Amsterdam, The Netherlands.

Van Rijn, L.C., Gaweesh, M.T.K., 1992. New total sediment-load sampler. Journal of Hydraulic Engineering 118, 1686–1691.

Zimmerman, J.T.F., 1981. Dynamics, diffusion and geomorphological significance of tidal residual eddies. Nature 290, 549–555.